Midlatitude Oceanic Fronts Strengthen the Moisture Transport from Anticyclones to Cyclones

Satoru Okajima[1], Hisashi Nakamura[2], and Thomas Spengler[3]

[1]The University of Tokyo
[2]University of Tokyo
[3]University of Bergen

October 17, 2023

Abstract

The Kuroshio-Oyashio Extension and Gulf Stream oceanic frontal zones with sharp sea-surface temperature gradients are characterized by enhanced activity of synoptic-scale cyclones and anticyclones and vigorous air-sea exchange of heat and moisture in the cold season. However, the air-sea exchanges attributed separately to cyclones and anticyclones have not been assessed. Here we quantify cyclonic and anticyclonic contributions around the oceanic frontal zones to surface turbulent heat fluxes, precipitation, and the associated hydrological cycle. The evaluation reveals that precipitation exceeds evaporation climatologically within cyclonic domains while evaporation dominates within anticyclonic domains. These features as well as the net moisture transport from anticyclonic to cyclonic domains are all enhanced in the presence of the frontal zones. Oceanic frontal zones thus climatologically act to strengthen the hydrological cycle through increasing low-level storm-track activity and specific humidity. These findings aid our understanding of the relationship between midlatitude air-sea interactions on synoptic- and longer-time scales.

Hosted file

972800_0_art_file_11450998_s1zmtz.docx available at https://authorea.com/users/601690/articles/671369-midlatitude-oceanic-fronts-strengthen-the-moisture-transport-from-anticyclones-to-cyclones

Midlatitude Oceanic Fronts Strengthen the Moisture Transport from Anticyclones to Cyclones

S. Okajima[1], H. Nakamura[1], and T. Spengler[2]

[1]Research Center for Advanced Science and Technology, The University of Tokyo, Tokyo, Japan

[2]Geophysical Institute, University of Bergen, and Bjerknes Centre for Climate Research, Bergen, Norway

Corresponding author: Satoru Okajima (okajima@atmos.rcast.u-tokyo.ac.jp)

Key Points:

- Cyclonic and anticyclonic contributions to air-sea heat and moisture exchange are quantified around midlatitude oceanic frontal zones
- Oceanic frontal zones primarily enhance surface turbulent heat fluxes within anticyclones and precipitation within cyclones, respectively
- Midlatitude oceanic frontal zones strenghen the net moisture transport from anticyclones to cyclones

Abstract

The Kuroshio-Oyashio Extension and Gulf Stream oceanic frontal zones with sharp sea-surface temperature gradients are characterized by enhanced activity of synoptic-scale cyclones and anticyclones and vigorous air-sea exchange of heat and moisture in the cold season. However, the air-sea exchanges attributed separately to cyclones and anticyclones have not been assessed. Here we quantify cyclonic and anticyclonic contributions around the oceanic frontal zones to surface turbulent heat fluxes, precipitation, and the associated hydrological cycle. The evaluation reveals that precipitation exceeds evaporation climatologically within cyclonic domains while evaporation dominates within anticyclonic domains. These features as well as the net moisture transport from anticyclonic to cyclonic domains are all enhanced in the presence of the frontal zones. Oceanic frontal zones thus climatologically act to strengthen the hydrological cycle through increasing low-level storm-track activity and specific humidity. These findings aid our understanding of the relationship between midlatitude air-sea interactions on synoptic- and longer-time scales.

Plain Language Summary

Two regions with pronounced sea surface temperature gradients over the North Pacific and North Atlantic are known as major oceanic frontal zones that are important for air-sea interactions with vigorous heat and moisture release from the ocean to the atmosphere. Recent studies found that high-frequency variations, such as migratory cyclones and anticyclones, are essential for the air-sea interaction over these frontal zones. However, the relative importance of cyclones and anticyclones has not been quantified. We show that anticyclonic contributions are important for the enhanced heat and moisture supply from the ocean in response to realistic oceanic frontal zones, while cyclonic contributions are crucial for the changes in rainfall. We further demonstrate that the moisture transport from anticyclones to cyclones is strengthened climatologically with the sharpness of midlatitude oceanic frontal zones. Our findings indicate that synoptic-scale migratory cyclones and anticyclones play an important role in midlatitude air-sea interactions. These results bridge the gap between our understanding of midlatitude air-sea interactions from day-to-day to longer-time scales.

1 Introduction

Midlatitude oceanic frontal zones that form along confluent warm and cool ocean currents with sharp meridional gradients in sea surface temperature (SST) are characterized by vigorous heat and moisture release from the ocean that can mainly be attributed to synoptic time scales (e.g., Ogawa and Spengler, 2019). In particular, the Kuroshio−Oyashio Extension (KOE) and Gulf Stream (GS) frontal zones are well known for their prominent heat release and restoring effect on near-surface baroclinicity (Tanimoto, 2003; Small et al., 2008; Nonaka et al., 2009; Kwon et al., 2010; Kelly et al., 2010; Papritz and Spengler, 2015; Czaja et al., 2019). Thereby, these frontal zones influence the climatological-mean surface wind convergence, precipitation, storm-tracks, atmospheric fronts, and westerly jets (e.g., Chelton et al., 2004; Nakamura et al., 2004, 2008; Minobe et al., 2008; Woollings et al., 2010; Parfitt et al., 2016; Ma et al., 2017; O'Neill et al, 2017; Masunaga et al., 2018, 2020a, 2020b; Reeder et al., 2021). They also have the potential to force basin-scale atmospheric anomalies and variabilities on interannual to decadal timescales (Taguchi et al., 2012; Okajima et al., 2014, 2018; Smirnov et al., 2015; O'Reilly and Czaja, 2015; O'Reilly et al., 2017). Recently, there has been mounting evidence that heat and moisture supplied in the midlatitudes are important for blocking events (Woollings, 2011; O'Reilly et al., 2016; Yamamoto et al., 2021) and intense warm moist intrusions into the Arctic (Woods et al., 2013; Papritz et al., 2021) that contribute to the pronounced warming trend over the Arctic (Woods and Cabarello, 2016; Gong et al., 2017; Messori et al., 2018). Nevertheless, the processes related to the vigorous supply of heat and moisture over the oceanic frontal zones as well as the transport and variability of the supplied heat and moisture on synoptic and longer time scales are not well understood.

Ogawa and Spengler (2019) highlighted the importance of wind variations on synoptic time scales in air-sea heat exchange over oceanic frontal zones. With a set of atmospheric general circulation model (AGCM) experiments, Kuwano-Yoshida and Minobe (2017) demonstrated that the KOE fronts act to enhance the intensification rate of migratory cyclones over the western North Pacific (NP), leading to a meandering jet over the eastern NP. To pinpoint the synoptic-scale processes relevant to the frontal air-sea interactions, Tsopouridis et al. (2021; hereafter TSS21) evaluated the surface flux contribution within extratropical cyclones to surface fluxes and assessed the impact of oceanic fronts over the NP and North Atlantic (NA). They found that extratropical cyclones are mainly important for a response in precipitation and only play a secondary role in modulating a response in surface turbulent heat fluxes (THF).

However, as the attribution of atmospheric fields to extratropical cyclones by TSS21 is based on a fixed-size circular mask centered on the position of a surface cyclone, their analysis does neither represent the actual size of different cyclones nor capture their three-dimensional structure. Furthermore, TSS21 did not assess the potential contribution of anticyclones. Hence, we still lack insight into the relative contributions of cyclones and anticyclones, which limits our understanding of midlatitude air-sea interactions around oceanic frontal zones.

Recently, Okajima et al. (2021; hereafter ONK21) proposed a method to quantify contributions from cyclonic and anticyclonic domains to Eulerian statistics, demonstrating that instantaneous local curvature can be used to distinguish low-level migratory cyclones and anticyclones as well as upper-level pressure troughs and ridges. We apply the ONK21 methodology to a set of AGCM experiments with observed climatological-mean and artificially smoothed SST fields to quantify the cyclonic and anticyclonic contributions to THF and precipitation along the two major oceanic frontal zones over the NP and NA. Our results provide insights into the hydrological cycle along the SST front as well as into the moisture exchange between cyclones and anticyclones.

2 Data and Methods

2.1 AGCM experiments

We analyze the same 6-hourly outputs of the AGCM experiments as analyzed by TSS21. The AGCM is the version 3 of the AGCM for the Earth Simulator (AFES; Ohfuchi et al., 2004; Enomoto et al., 2008; Kuwano-Yoshida et al., 2010). The data period spans from 1 September 1981 to 31 August 2001 with a horizontal resolution of ~0.5° (T239) and 48 vertical levels. In the control experiment (CNTL), the climatological-mean SST derived from the 0.25° daily OISST (Reynolds et al., 2007) was prescribed. In the SMTHK and SMTHG experiments, the prescribed SST fields have been horizontally smoothed over the western NP and NA, respectively. Responses to the realistic KOE and GS fronts can be evaluated as the difference between the corresponding smoothed experiments and CNTL (i.e., CNTL−SMTHK and CNTL−SMTHG, respectively). Figures 1a-b show the differences in SST prescribed to CNTL compared to SMTHK and SMTHG, respectively.

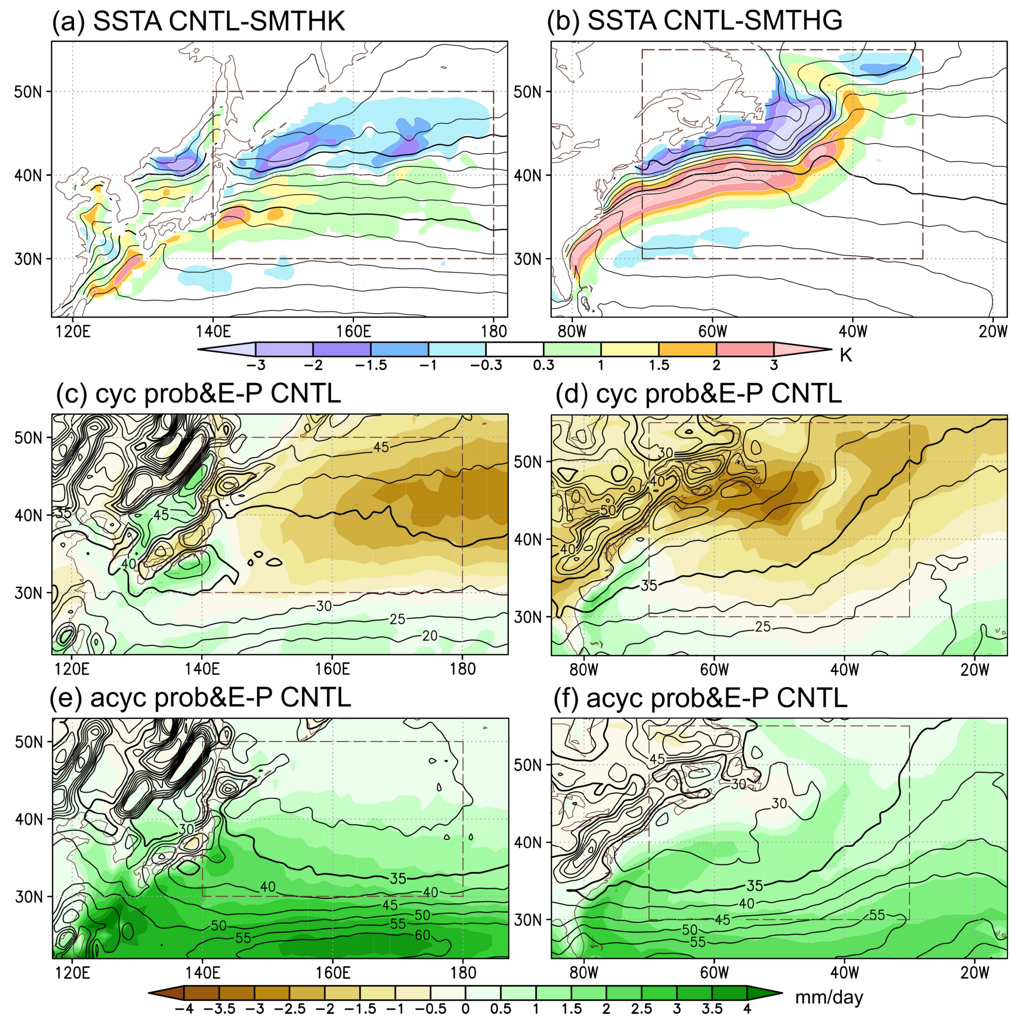

Figure 1. **a-b** Mean and its differences in SST (shading in K) from (a) SMTHK and (b) SMTHG wintertime SST prescribed for CNTL (contour every 2K, thick for every 10K). Climatological cyclonic contribution to E−P (shading in mm/day) in CNTL over the (c) NP and (d) NA and climatological probability of cyclonic domains (contours every 5%, thick for 35%). **e-f** Same as in c-d, respectively, but for the anticyclonic contributions and probabilities. Dashed boxes signify the domains in which the area-averaged contributions are calculated separately for the NP and NA.

We focus on wintertime (DJF) mean responses following TSS21. Statistical significance is assessed by a Student's *t*-test. In section 3.3, we calculate area-averaged THF, precipitation, and E−P within the oceanic frontal zones over the NP [140°E−180°, 30°−50°N] and the NA [70°−30°W, 30°−55°N] to focus on regions of active synoptic-scale eddies, using the data only at grid points over the ocean. Hereafter, a positive value of THF indicates an upward flux.

2.2 Separating contributions from cyclonic and anticyclonic domains

We determine cyclonic and anticyclonic domains by evaluating the two-dimensional curvature of the horizontal wind (see ONK21). We calculate the climatological contribution of a given variable by accumulating its instantaneous values within cyclonic or anticyclonic domains, normalized by the total number of times steps, to yield additive climatological contributions. For evaporation (E), we use surface latent heat fluxes and assume a latent heat of vaporization of 2,500 kJ/kg.

We did not smooth the data horizontally to retain the influence of the land surface at a minimum. We use the curvature of wind at 850-hPa to determine our cyclonic and anticyclonic domains, because near-surface wind is likely to be influenced by underlyng SST directly through vertical mixing (Wallace et al., 1989; Hayes et al., 1989) or pressure adjustment mechanism (Lindzen and Nigam, 1987), which makes it rather difficult to extract the contributions from synoptic-scale cyclones and anticyclones.

We set a curvature threshold of $\pm 4.0 \times 10^{-6}\ \mathrm{m}^{-1}$ to determine cyclonic and anticyclonic domains, respectively, corresponding to a curvature radius of 2,500 km. Grid points with a curvature radius larger than the threshold are named "neutral", because they are classified neither as "cyclonic" nor as "anticyclonic". Our results are not very sensitive to setting the curvature threshold to zero (Supplementary Fig. S1) or $\pm 1.0 \times 10^{-5}\ \mathrm{m}^{-1}$ (Supplementary Fig. S2). We also obtain similar results based on the curvature of wind at 925-hPa (Supplementary Fig. S3).

Overall, we obtain qualitatively similar results to CNTL based on the JRA-55 reanalysis (Text S1 and Supplementary Figs. S4, S6, and S8).

3 Results

3.1 Cyclonic and anticyclonic contributions to the climatological hydrological cycle for CNTL

Over both oceanic frontal zones in the NP and NA, the cyclonic contribution to the climatological difference between evaporation minus precipitation (E–P) is overall negative (Figs. 1c-d), indicative of excessive precipitation compared to local evaporation within cyclonic domains in the storm-track core regions. In the storm-track entrance regions, a positive cyclonic E–P contribution is evident over the ocean, especially along the Kuroshio Current south of Japan and the Florida Current by Cape Hatteras.

In contrast, the anticyclonic contribution to the climatological E–P is overall positive (Figs. 1e-f), especially equatorward of the storm-track cores and along the warm ocean currents. The large anticyclonic E–P contribution south of ~30–35°N is most likely related to the relatively high probability of anticyclonic domains (ONK21). The difference between the distributions of the cyclonic and anticyclonic frequencies is compatible with those of the densities of migratory cyclones and anticyclones based on Lagrangian tracking (Hoskins and Hodges, 2002; Okajima et al., 2023). In the storm-track entrance regions, the large positive anticyclonic E–P contribution is indicative of the importance of cold-air outbreaks for air-sea heat exchange in those regions, which acts as thermal damping for transient eddy activity (Okajima et al., 2022).

3.2 Local response of the climatological-mean hydrological cycle to oceanic frontal zones

In response to changes in the NP oceanic frontal zone, the cyclonic contribution to the climatological E–P significantly decreases, especially over the cool SST anomalies along the main branch of the Oyashio Front and the front over the Japan Sea (Figs. 1a and 2a). In the former region, this response acts to enhance the climatological-mean precipitation excess by up to ~30% (Fig. 1c), with no apparent change in the frequency of cyclonic domains around the oceanic frontal zone (Fig. 2a). In the latter region, the climatological-mean excess in evaporation is reduced substantially together with a slight decrease in the occurrence of cyclonic domains. In addition, the weaker negative cyclonic contribution to the E–P response around the second branch of the Oyashio Front (around 40°N, 170°E) is likely associated with a decreased occurrence of cyclonic domains, which is consistent with the cyclone density response in TSS21. Over the warm SST anomaly around the Kuroshio Extension, however, the cyclonic contribution to E–P does not significantly change in response to the oceanic frontal zone.

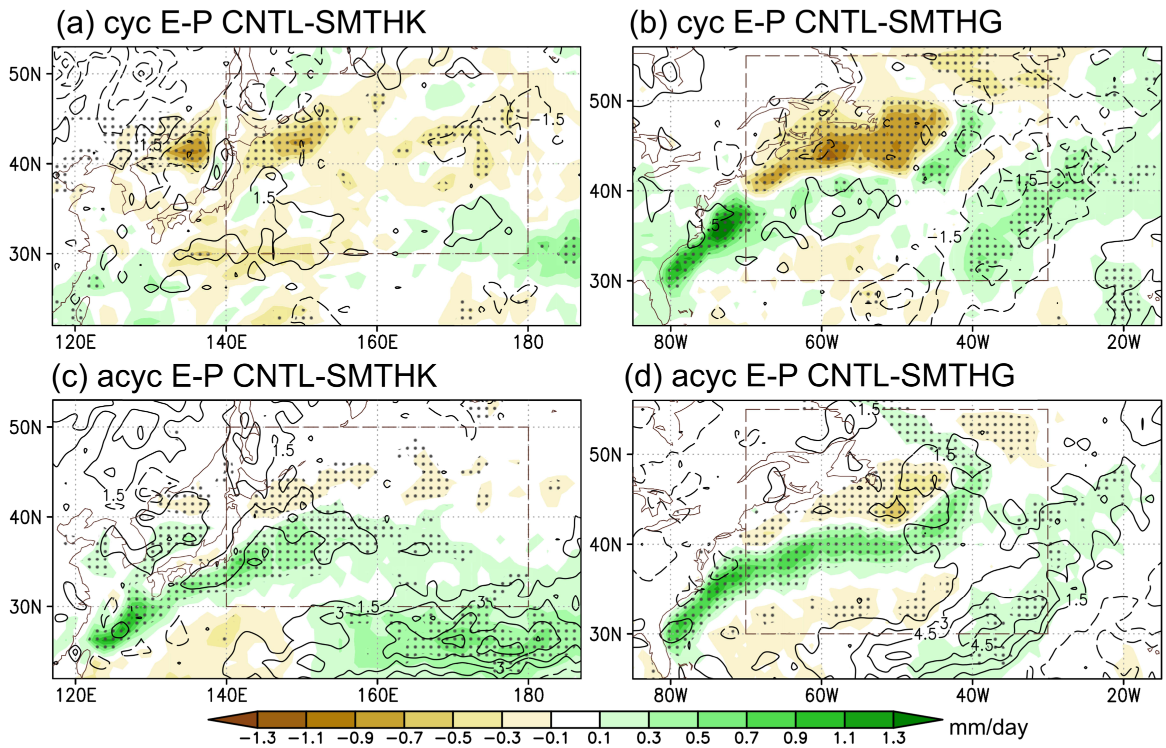

Figure 2. **a** Cyclonic contribution to the response (CNTL−SMTHK) of the climatological E−P (shadings in mm/day). Stipples signify statistically significant signals at the 90% confidence level by a Student's *t*-test. Contours denote the cyclonic contribution to the probability of cyclonic domains (every 1.5%, zero contours omitted; dashed for negative values). **b** Same as in a, but for CNTL−SMTHG. **c-d** Same as in a-b, but for the anticyclonic contributions and probabilities. Dashed boxes signify the domains within which area-averaged contributions are calculated separately for the NP and NA.

Over oceanic frontal zone in the NA, the negative cyclonic contribution to the E–P response is even more evident over the pronounced cool SST anomaly on the poleward flank of the GS (Fig. 2b). The positive cyclonic contribution to the E–P response over the warm SST anomaly is overall modest, but it is marked along the GS just off the U.S. east coast, where the enhancement of THF dominates over the precipitation increase (Supplementary Fig. S5). These cyclonic E–P responses are not associated with changes in the occurrence of cyclonic domains. However, the positive cyclonic E–P contribution in the central NA(~30–40°W) is most likely associated with a decrease in the occurrence of cyclonic domains, which is consistent with TSS21.

Conversely, the anticyclonic contribution to the climatological positive E–P is significantly enhanced (by ~20–40%) in response to the NP and NA oceanic fronts, especially over the warm ocean currents and SST anomalies equatorward of them (Figs. 1c-d and 2a-b). Meanwhile, the negative contribution to the E–P response over the cool SST anomalies is substantially weaker than the decrease in cyclonic contribution to the E–P counterpart along the main branch of the Oyashio Front and the front over the Japan Sea (Fig. 2a). The enhanced E–P within anticyclonic domains is due partly to the increased occurrence of anticyclonic domains, especially around the NP oceanic frontal zones (Fig. 2c). The occurrence of anticyclonic domains also increases in the climatological anticyclones southeast of the respective oceanic frontal zones.

The differences between the cyclonic and anticyclonic contributions to the E–P response to the oceanic frontal zones are related to responses in both THF and precipitation (Supplementary Fig. S5). Within cyclonic domains, the suppression of upward THF over the cool SST anomalies as well as the pronounced precipitation increase over the warm SST anomalies yield the overall negative contribution to the E–P response for the cyclonic domains, whereas the corresponding anticyclonic response in precipitation is weaker. The anticyclonic contribution to the THF response is somewhat greater than the cyclonic counterpart over the warm SST anomalies around the NP frontal zones and along the Kuroshio, while the opposite is the case over the warm SST anomalies along the GS.

3.3 Area-averaged, net contributions to the hydrological cycle

The area-averaged cyclonic contribution to the climatological-mean net (viz. sensible plus latent) THF is substantially (by ~30–50%) larger than its anticyclonic counterpart over both the NP and NA (Figs. 3a-b). The contribution of neutral domains to THF is roughly comparable with the cyclonic or anticyclonic contributions, with the three types of domains being comparably probable (Figs. 1c-f). The substantial THF contribution of neutral domains is compatible with the importance of cyclone-anticyclone transition zones, as pointed out by Rudeva and Gulev (2011) and Tilinina et al. (2018). In contrast, the climatological-mean total precipitation is associated predominantly with cyclonic domains (Figs. 3a-b). The additional contribution from neutral domains may be associated with atmospheric fronts, cold-air outbreaks, or planetary waves. The climatological E–P is positive (negative) for anticyclonic (cyclonic) domains, indicative of their distinct roles in the climatological hydrological cycle (see section 3.1). Neutral domains also contribute positively to the E–P climatology. The result is consistent with that based on the JRA-55 (Supplementary Fig. S6).

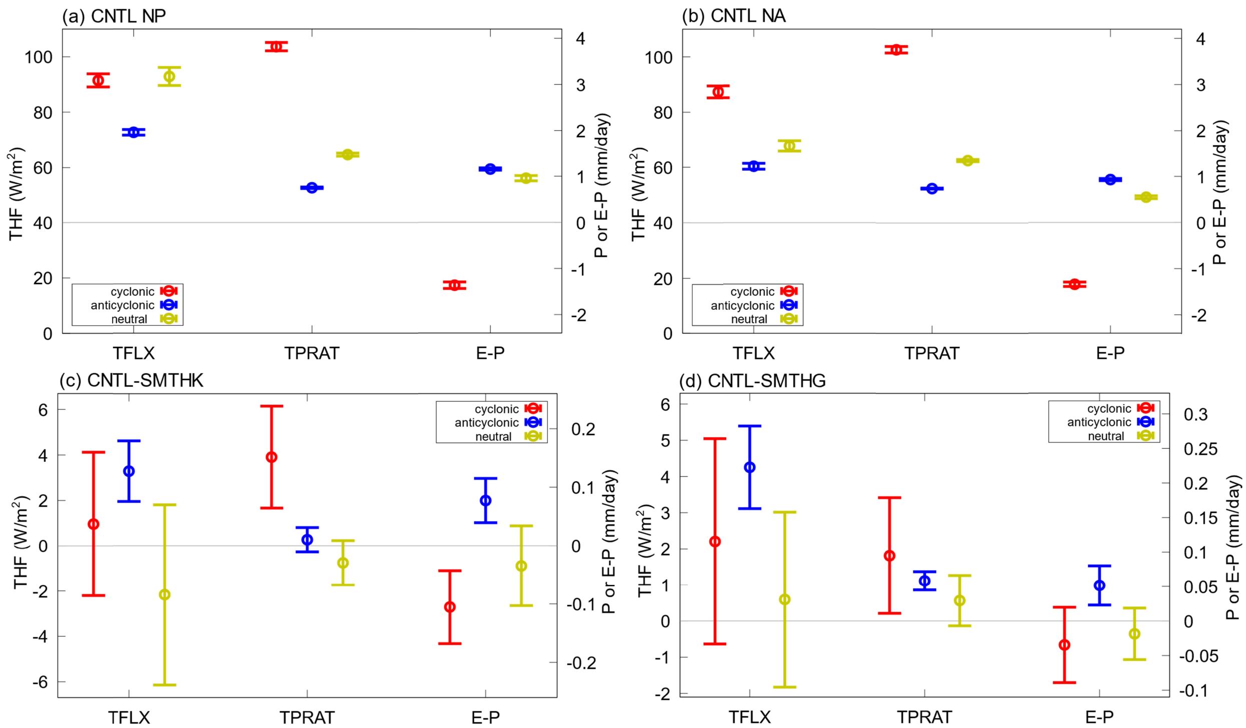

Figure 3. **a** Area-averaged climatological-mean net turbulent heat flux (W/m^2), total precipitation (mm/day), and E–P (mm/day) over the NP frontal region (rectangular domain marked in Fig. 1) based on CNTL. Red, blue, and yellow bars represent the contributions from cyclonic, anticyclonic, and neutral (neither cyclonic nor anticyclonic) domains, respectively. Whiskers signify standard errors. **b** Same as in a, but for the NA frontal region. **c-d** Same as in a-b, respectively, but for the response to oceanic frontal zones as extracted in (c) CNTL−SMTHK and (d) CNTL−SMTHG.

The oceanic frontal zones significantly increase the anticyclonic contribution to the area-averaged climatological THF over the NP and NA (Figs. 3c-d). The corresponding response of the cyclonic THF contribution is weaker than the anticyclonic counterpart, especially over the NP (Fig. 3c). This suggests the significance of anticyclones in the restoration of near-surface baroclinicity, which is essential for storm-track maintenance (e.g., Nakamura et al., 2004, 2008; Nonaka et al., 2009; Taguchi et al., 2009; Hotta and Nakamura, 2011; Papritz and Spengler, 2015). Meanwhile, the oceanic frontal zones significantly amplify the cyclonic contribution to the area-averaged climatological precipitation over the NP and NA (Figs. 3c-d). Over the NA, precipitation is enhanced slightly also within anticyclonic and neutral domains (Fig. 3d), which may be associated with atmospheric fronts and cold-air outbreaks. Those cyclonic contributions to the THF and precipitation responses are compatible with TSS21.

As a net response of the hydrological cycle to the realistic oceanic frontal zones, the climatological E–P increases and decreases within anticyclonic and cyclonic domains, respectively (Figs. 3c-d), with an insignificant negative E–P contribution from neutral domains. This indicates that the respective climatological-mean positive and negative E–P contributions of anticyclonic and cyclonic domains are strengthened by the oceanic frontal zones. Note that the relative roles of the cyclonic and anticyclonic contributions to the E–P response are not affected qualitatively by the corresponding response of the probability of cyclonic and anticyclonic domains (Supplementary Fig. S7).

3.4 Moisture transport between cyclonic to anticyclonic domains

The preceding section suggests that the oceanic frontal zones enhance the moisture supply from the ocean mainly within anticyclonic domains with an implied transport into cyclonic domains. To verify this, we calculate the moisture flux projected onto the upgradient direction of local curvature, which points to positive cyclonic curvature. We use this projected flux through cyclone-anticyclone transition zones as a measure of the net moisture transport from cyclonic domains to anticyclonic domains (see Text S2 for details).

The climatological net moisture transport through cyclone-anticyclone transition zones in CNTL is overall positive for both the NP and NA (Figs. 4a-b), indicative of the net moisture transport from anticyclonic to cyclonic domains. This is consistent with the results obtained in section 3.3 and the results based on the JRA-55 (Supplementary Fig. S8). This result is also compatible with Bui and Spengler (2021), who suggested the importance of feeding airstreams taking up moisture ahead of a cyclone. The moisture transport is particularly strong equatorward of the precipitation maxima (Figs. 4a-b), over which the climatological-mean evaporation tends to be larger than precipitation.

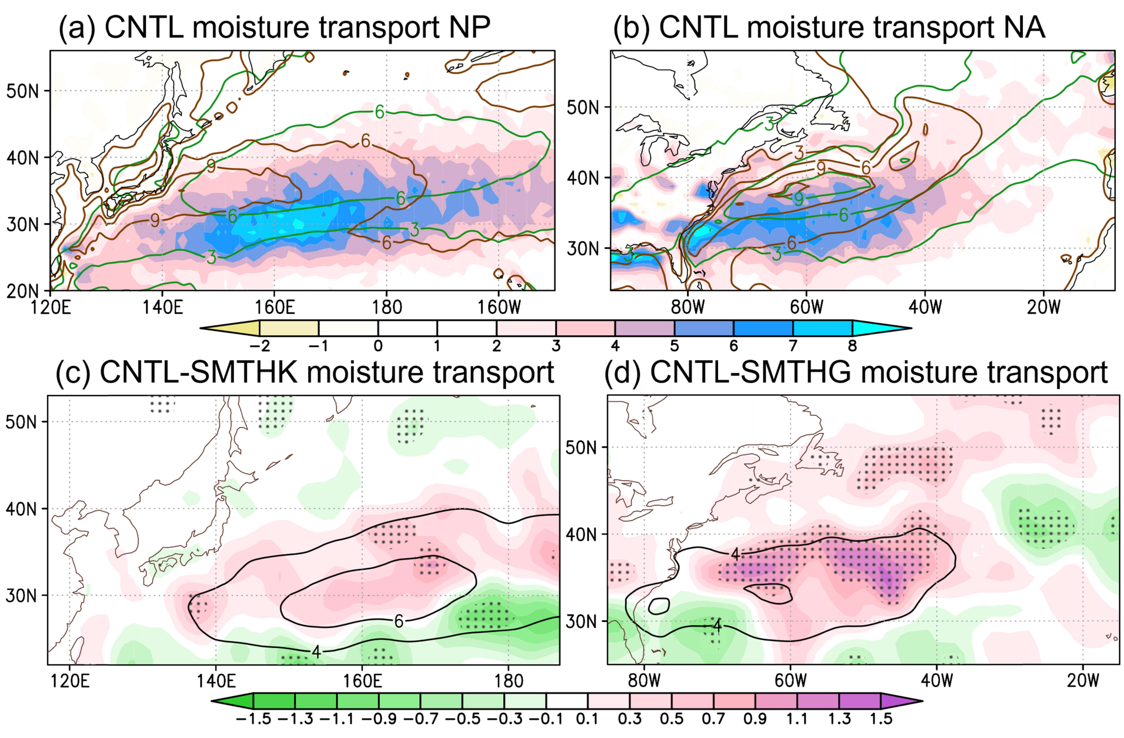

Figure 4. **a** Climatological-mean net moisture transport (from anticyclonic to cyclonic domains) integrated from the surface to 100 hPa (shading in mm m/s) over the NP for CNTL. Brown and green contours denote the climatological-mean evaporation and precipitation (mm/day), respectively. **b** Same as in a, but for the NA. **c-d** Same as in a-b, respectively, but for responses

for (c) CNTL−SMTHK and (d) CNTL−SMTHG. Stipples signify statistically significant signals at the 90% confidence level by a Student's *t*-test. Black contours indicate the climatological-mean moisture exchange (mm m/s) in CNTL (field smoothed).

The oceanic frontal zones strengthen the climatological cyclone-anticyclone moisture transport (Figs. 4c-d), which is compatible with the results of the E–P contributions (Figs. 3c-d). The more distinct enhancement in the moisture transport over the NA is most likely related to the stronger positive SST anomaly over the NA (Fig. 1b). Increased specific humidity around the warm ocean currents and positive SST anomalies equatorward of the oceanic frontal zones as well as intensified low-level storm-track activity are the most likely causes for the enhanced moisture transport (Supplementary Fig. S9).

4 Conclusions

We assessed the role of cyclones and anticyclones in air-sea interactions over midlatitude oceanic frontal zones in the wintertime Northern Hemisphere by quantifying cyclonic and anticyclonic contributions to the climatological THF, precipitation, and E–P as well as their responses to the oceanic frontal zones based on AGCM experiments. In addition, we delineated the climatological moisture transport between cyclonic and anticyclonic domains and their corresponding response to the influence of the SST fronts.

We demonstrated that synoptic-scale, sub-weekly disturbances play an important role in midlatitude air-sea interactions on a climatological time scale, bridging our understanding of midlatitude air-sea interactions from synoptic to longer time scales. When smoothing the SST gradients, THF is climatologically reduced when compared to realistic oceanic frontal zones. This reduction mainly occurs within anticyclonic domains, while precipitation is climatologically enhanced predominantly within cyclonic domains. Consistently, the net moisture transport from anticyclonic to cyclonic domains is strengthened when realistic oceanic frontal zones are present. These changes are mainly attributable to a moisture increase around the anomalously warmer waters as well as enhanced storm-track activity, yielding an overall strengthened climatological hydrological cycle around the midlatitude oceanic frontal zones.

Our results thus emphasize that variations in synoptic-scale THF and precipitation are modulated by midlatitude frontal zones and SSTs around them. The modulation of heat and moisture release along oceanic frontal zones can modulate storm-track activity and a westerly jet response (e.g., Nakamura et al., 2008; Kuwano-Yoshida and Minobe, 2017), though requires further studies to pinpoint the mechanisms including the enhancement of moisture transport from cyclones to anticyclones.

Acknowledgments

This study is supported in part by the Japanese Ministry of Education, Culture, Sports, Science and Technology (MEXT) through the Arctic Challenge for Sustainability (ArCS-II;

JPMXD1420318865) and through the advanced studies of climate change projection (SENTAN) Grant Number JPMXD0722680395, by the Japan Science and Technology Agency through COI-NEXT JPMJPF2013, by the Environmental Restoration and Conservation Agency of Japan through Environment Research and Technology Development Fund JPMEERF20222002, and by the Japan Society for the Promotion of Science (JSPS) through Grants-in-Aid for Scientific Research 19H05702 (on Innovative Areas 6102), 20H01970, 22H01292 and 22K14097. TS is supported by the BALMCAST project (324081) financed by the Research Council of Norway.

Open Research

The details of the model experiments analyzed in this study is described in Kuwano-Yoshida and Minobe (2017). The data of those experiments are available at https://doi.org/10.11582/2021.00075. Figures were produced using the Grid Analysis Display System (GrADS; http://cola.gmu.edu/grads/), gnuplot v5.2 (http://www.gnuplot.info), matplotlib v3.7.1 (https://matplotlib.org/stable/index.html), and Inkscape v1.0.1 (https://www.inkscape.org).

References

Bui, H., & Spengler, T. (2021). On the influence of sea surface temperature distributions on the development of extratropical cyclones. *Journal of the Atmospheric Sciences*, 78(4), 1173-1188.

Chelton, D. B., Schlax, M. G., Freilich, M. H., & Milliff, R. F. (2004). Satellite measurements reveal persistent small-scale features in ocean winds. *Science*, *303*(5660), 978–983.

Czaja, A., Frankignoul, C., Minobe, S., & Vannière, B. (2019). Simulating the midlatitude atmospheric circulation: What might we gain from high-resolution modeling of air-sea interactions? *Current Climate Change Reports*, *5*(4), 390–406.

Enomoto, T., Kuwano-Yoshida, A., Komori, N., & Ohfuchi, W. (2008). Description of AFES 2: Improvements for High-Resolution and Coupled Simulations. In K. Hamilton & W. Ohfuchi (Eds.), *High Resolution Numerical Modelling of the Atmosphere and Ocean* (pp. 77–97). New York, NY: Springer New York.

Gong, T., Feldstein, S., & Lee, S. (2017). The Role of Downward Infrared Radiation in the Recent Arctic Winter Warming Trend. *Journal of Climate*, *30*(13), 4937–4949.

Hayes, S. P., McPhaden, M. J., & Wallace, J. M. (1989). The influence of sea-surface temperature on surface wind in the eastern equatorial Pacific: Weekly to monthly variability. *Journal of Climate*, 2(12), 1500–1506.

Hotta, D., & Nakamura, H. (2011). On the significance of the sensible heat supply from the ocean in the maintenance of the mean baroclinicity along storm tracks. *Journal of Climate*, 24(13), 3377–3401.

Kelly, K. A., Small, R. J., Samelson, R. M., Qiu, B., Joyce, T. M., Kwon, Y.-O., & Cronin, M. F. (2010). Western boundary currents and frontal air–sea interaction: Gulf Stream and Kuroshio Extension. *Journal of Climate*, *23*(21), 5644–5667.

Kuwano-Yoshida, A., & Minobe, S. (2017). Storm-Track Response to SST Fronts in the Northwestern Pacific Region in an AGCM. *Journal of Climate*, *30*(3), 1081–1102.

Kuwano-Yoshida, A., Minobe, S., & Xie, S.-P. (2010). Precipitation Response to the Gulf Stream in an Atmospheric GCM. *Journal of Climate*, *23*(13), 3676–3698.

Kwon, Y.-O., Alexander, M. A., Bond, N. A., Frankignoul, C., Nakamura, H., Qiu, B., & Thompson, L. A. (2010). Role of the Gulf Stream and Kuroshio–Oyashio Systems in Large-

Scale Atmosphere–Ocean Interaction: A Review. *Journal of Climate*, *23*(12), 3249–3281.

Lindzen, R. S., & Nigam, S. (1987). On the role of sea surface temperature gradients in forcing low-level winds and convergence in the tropics. *Journal of the Atmospheric Sciences*, 44(17), 2418–2436.

Ma, X., Chang, P., Saravanan, R., Montuoro, R., Nakamura, H., Wu, D., et al. (2017). Importance of Resolving Kuroshio Front and Eddy Influence in Simulating the North Pacific Storm Track. *Journal of Climate*, *30*(5), 1861–1880.

Masunaga, R., Nakamura, H., Kamahori, H., Onogi, K., & Okajima, S. (2018). JRA-55CHS: An atmospheric reanalysis produced with high-resolution SST. *SOLA*, *14*, 6–13.

Masunaga, R., Nakamura, H., Taguchi, B., & Miyasaka, T. (2020a). Processes shaping the frontal-scale time-mean surface wind convergence patterns around the Kuroshio Extension in winter. *Journal of Climate*, 33(1), 3–25.

Masunaga, R., Nakamura, H., Taguchi, B., & Miyasaka, T. (2020b). Processes shaping the frontal-scale time-mean surface wind convergence patterns around the Gulf Stream and Agulhas Return Current in winter. *Journal of Climate*, 33(21), 9083–9101.

Messori, G., Woods, C., & Caballero, R. (2018). On the drivers of wintertime temperature extremes in the high Arctic. *Journal of Climate*, *31*(4), 1597-1618.

Minobe, S., Kuwano-Yoshida, A., Komori, N., Xie, S.-P., & Small, R. J. (2008). Influence of the Gulf Stream on the troposphere. *Nature*, *452*(7184), 206–209.

Nakamura, H., Sampe, T., Tanimoto, Y., & Shimpo, A. (2004). Observed associations among storm tracks, jet streams and midlatitude oceanic fronts. *Earth's Climate: The Ocean--Atmosphere Interaction, Geophys. Monogr*, *147*, 329–345.

Nakamura, H., Sampe, T., Goto, A., Ohfuchi, W., & Xie, S.-P. (2008). On the importance of midlatitude oceanic frontal zones for the mean state and dominant variability in the tropospheric circulation. *Geophysical Research Letters*, *35*, L15709.

Nonaka, M., Nakamura, H., Taguchi, B., Komori, N., Kuwano-Yoshida, A., & Takaya, K. (2009). Air–sea heat exchanges characteristic of a prominent midlatitude oceanic front in the South Indian Ocean as simulated in a high-resolution coupled GCM. *Journal of Climate*, *22*(24), 6515–6535.

O'Neill, L. W., Haack, T., Chelton, D. B., & Skyllingstad, E. (2017). The Gulf Stream convergence zone in the time-mean winds. *Journal of the Atmospheric Sciences*, 74(7), 2383-2412.

O'Reilly, C. H., & Czaja, A. (2015). The response of the Pacific storm track and atmospheric circulation to Kuroshio Extension variability. *Quarterly Journal of the Royal Meteorological Society*, *141*(686), 52–66.

O'Reilly, C. H., Minobe, S., & Kuwano-Yoshida, A. (2016). The influence of the Gulf Stream on wintertime European blocking. *Climate Dynamics*, *47*(5-6), 1545–1567.

O'Reilly, C. H., Minobe, S., Kuwano-Yoshida, A., & Woollings, T. (2017). The Gulf Stream influence on wintertime North Atlantic jet variability. *Quarterly Journal of the Royal Meteorological Society*, *143*(702), 173–183.

Ogawa, F., & Spengler, T. (2019). Prevailing Surface Wind Direction during Air–Sea Heat Exchange. *Journal of Climate*, *32*(17), 5601–5617.

Ohfuchi, W., Nakamura, H., Yoshioka, M. K., Enomoto, T., Takaya, K., Peng, X., et al. (2004). 10-km mesh meso-scale resolving simulations of the global atmosphere on the Earth Simulator:

Preliminary outcomes of AFES (AGCM for the Earth Simulator). *Journal of the Earth Simulator*, *1*, 8-34.

Okajima, S., Nakamura, H., Nishii, K., Miyasaka, T., & Kuwano-Yoshida, A. (2014). Assessing the importance of prominent warm SST anomalies over the midlatitude North Pacific in forcing large-scale atmospheric anomalies during 2011 summer and autumn. *Journal of Climate*, *27*(11), 3889–3903.

Okajima, S., Nakamura, H., Nishii, K., Miyasaka, T., Kuwano-Yoshida, A., Taguchi, B., et al. (2018). Mechanisms for the Maintenance of the Wintertime Basin-Scale Atmospheric Response to Decadal SST Variability in the North Pacific Subarctic Frontal Zone. *Journal of Climate*, *31*(1), 297–315.

Okajima, S., Nakamura, H., & Kaspi, Y. (2021). Cyclonic and anticyclonic contributions to atmospheric energetics. *Scientific Reports*, *11*(1), 13202.

Okajima, S., Nakamura, H., & Kaspi, Y. (2022). Energetics of transient eddies related to the midwinter minimum of the North Pacific storm-track activity. *Journal of Climate*, *35*(4), 1137–1156.

Okajima, S., Nakamura, H., & Kaspi, Y. (2023). Distinct roles of cyclones and anticyclones in setting the midwinter minimum of the North Pacific eddy activity: a Lagrangian perspective. *Journal of Climate*, 36(14), 4793–4814.

Papritz, L., Aemisegger, F., & Wernli, H. (2021). Sources and transport pathways of precipitating waters in cold-season deep North Atlantic cyclones. *Journal of the Atmospheric Sciences*, *78*(10), 3349–3368.

Parfitt, R., Czaja, A., Minobe, S., & Kuwano-Yoshida, A. (2016). The atmospheric frontal response to SST perturbations in the Gulf Stream region. *Geophysical Research Letters*, *43*(5), 2299–2306.

Reynolds, R. W., Smith, T. M., Liu, C., Chelton, D. B., Casey, K. S., & Schlax, M. G. (2007). Daily High-Resolution-Blended Analyses for Sea Surface Temperature. *Journal of Climate*, *20*(22), 5473–5496.

Reeder, M. J., Spengler, T., & Spensberger, C. (2021). The effect of sea surface temperature fronts on atmospheric frontogenesis. *Journal of the Atmospheric Sciences*, 78(6), 1753–1771.

Rudeva, I., & Gulev, S. K. (2011). Composite Analysis of North Atlantic Extratropical Cyclones in NCEP–NCAR Reanalysis Data. *Monthly Weather Review*, *139*(5), 1419–1446.

Small, R. J., deSzoeke, S. P., Xie, S. P., O'Neill, L., Seo, H., Song, Q., et al. (2008). Air–sea interaction over ocean fronts and eddies. *Dynamics of Atmospheres and Oceans*, *45*(3), 274–319.

Smirnov, D., Newman, M., Alexander, M. A., Kwon, Y.-O., & Frankignoul, C. (2015). Investigating the Local Atmospheric Response to a Realistic Shift in the Oyashio Sea Surface Temperature Front. *Journal of Climate*, *28*(3), 1126–1147.

Taguchi, B., Nakamura, H., Nonaka, M., Komori, N., Kuwano-Yoshida, A., Takaya, K., & Goto, A. (2012). Seasonal evolutions of atmospheric response to decadal SST anomalies in the North Pacific subarctic frontal zone: Observations and a coupled model simulation. *Journal of Climate*, *25*(1), 111–139.

Taguchi, B., Nakamura, H., Nonaka, M., & Xie, S. P. (2009). Influences of the Kuroshio/Oyashio Extensions on air–sea heat exchanges and storm-track activity as revealed in regional atmospheric model simulations for the 2003/04 cold season. *Journal of Climate*, 22(24), 6536–6560.

Tanimoto, Y. (2003). An active role of extratropical sea surface temperature anomalies in determining anomalous turbulent heat flux. *Journal of Geophysical Research*, *108*(C10).

Tilinina, N., Gavrikov, A., & Gulev, S. K. (2018). Association of the North Atlantic Surface Turbulent Heat Fluxes with Midlatitude Cyclones. *Monthly Weather Review*, *146*(11), 3691–3715.

Tsopouridis, L., Spengler, T., & Spensberger, C. (2021). Smoother versus sharper Gulf Stream and Kuroshio sea surface temperature fronts: effects on cyclones and climatology. *Weather and Climate Dynamics*, *2*(4), 953–970.

Wallace, J. M., Mitchell, T. P., & Deser, C. (1989). The influence of sea-surface temperature on surface wind in the eastern equatorial Pacific: Seasonal and interannual variability. *Journal of Climate*, 2(12), 1492–1499.

Woods, C., & Caballero, R. (2016). The role of moist intrusions in winter Arctic warming and sea ice decline. *Journal of Climate*, *29*(12), 4473–4485.

Woods, C., Caballero, R., & Svensson, G. (2013). Large-scale circulation associated with moisture intrusions into the Arctic during winter. *Geophysical Research Letters*, *40*(17), 4717–4721.

Woollings, T. (2011). Ocean effects of blocking. *Science*, *334*, 612–613.

Woollings, T., Hoskins, B., Blackburn, M., Hassell, D., & Hodges, K. (2010). Storm track sensitivity to sea surface temperature resolution in a regional atmosphere model. *Climate Dynamics*, *35*(2), 341–353.

Yamamoto, A., Nonaka, M., Martineau, P., Yamazaki, A., Kwon, Y. O., Nakamura, H., & Taguchi, B. (2021). Oceanic moisture sources contributing to wintertime Euro-Atlantic blocking. *Weather and Climate Dynamics*, 2(3), 819–840.

Geophysical Research Letters

Supporting Information for

Midlatitude Oceanic Fronts Strengthen the Moisture Transport from Anticyclones to Cyclones

S. Okajima[1], H. Nakamura[1], and T. Spengler[2]

[1]Research Center for Advanced Science and Technology, The University of Tokyo, Tokyo, Japan

[2]Geophysical Institute, University of Bergen, and Bjerknes Centre for Climate Research, Bergen, Norway

Contents of this file

Introduction

The supporting information includes (1) two text sections that describe details of the JRA-55 reanalysis and how to evaluate moisture transport locally between cyclonic and anticyclonic domains, and (2) nine supplementary figures that are referred to but not presented in the main text.

Text S1.

To verify the reproducibility of CNTL, we utilize the global atmospheric JRA-55 reanalysis (Kobayashi et al. 2015; Harada et al. 2016) in Supplementary Figs. S4 and S7 to compare the climatological-mean fields with those from CNTL. We analyze 6-hourly fields of surface sensible and latent heat fluxes as well as precipitation for the period 1958/59-2019/20. The JRA-55 has been constructed by the Japan Meteorological Agency (JMA) through a four-dimensional variational data assimilation system with TL319 horizontal resolution (equivalent to 55 km) and 60 vertical levels up to 0.1-hPa.

Harada, Y., Kamahori, H., Kobayashi, C., Endo, H., Kobayashi, S., Ota, Y., et al. (2016). The JRA-55 Reanalysis: Representation of Atmospheric Circulation and Climate Variability. *Journal of the Meteorological Society of Japan*, 94(3), 269–302.
Kobayashi, S., Ota, Y., Harada, Y., Ebita, A., Moriya, M., Onoda, H., et al. (2015). The JRA-55 Reanalysis: General specifications and basic characteristics. *Journal of the Meteorological Society of Japan*, 93(1), 5–48.

Text S2.

As a measure of moisture transport between cyclonic and anticyclonic domains, we calculated a moisture flux projected onto the upgradient direction of local curvature. Under the assumption of a geostrophic wind balance, the upgradient direction of local curvature is normal to horizontal wind vector pointing to a larger cyclonic curvature.

Specifically, the scaler value is evaluated at each pressure level as:

$$\epsilon \equiv (q\mathbb{v}') \cdot \frac{\nabla\kappa_2}{|\nabla\kappa_2|},$$

where $\mathbb{v}$ denotes horizontal wind, q specific humidity, κ_2 two-dimensional curvature of the wind vectors, and a prime high-pass-filtered fluctuations based on a Lanczos filter with a cutoff period of 8 days. Here, the moisture flux was calculated with high-pass-filtered wind fluctuations to measure the effectiveness of moisture transport associated with transient eddies, in analogy to (anti)cyclone-relative winds. Nevertheless, we have confirmed that a qualitatively similar result can be obtained with fluctuations calculated either with unfiltered horizontal wind components or with high-pass-filtered specific humidity. We calculated the climatological-mean value of ϵ with a mask of grid points where the local curvature radius is less than 2,500km to focus on marginal zones between cyclonic and anticyclonic domains where the moisture transport takes place. The moisture transport shown in Fig. 4 and Supplementary Fig. S8 is vertically integrated from the surface to the 100-hPa.

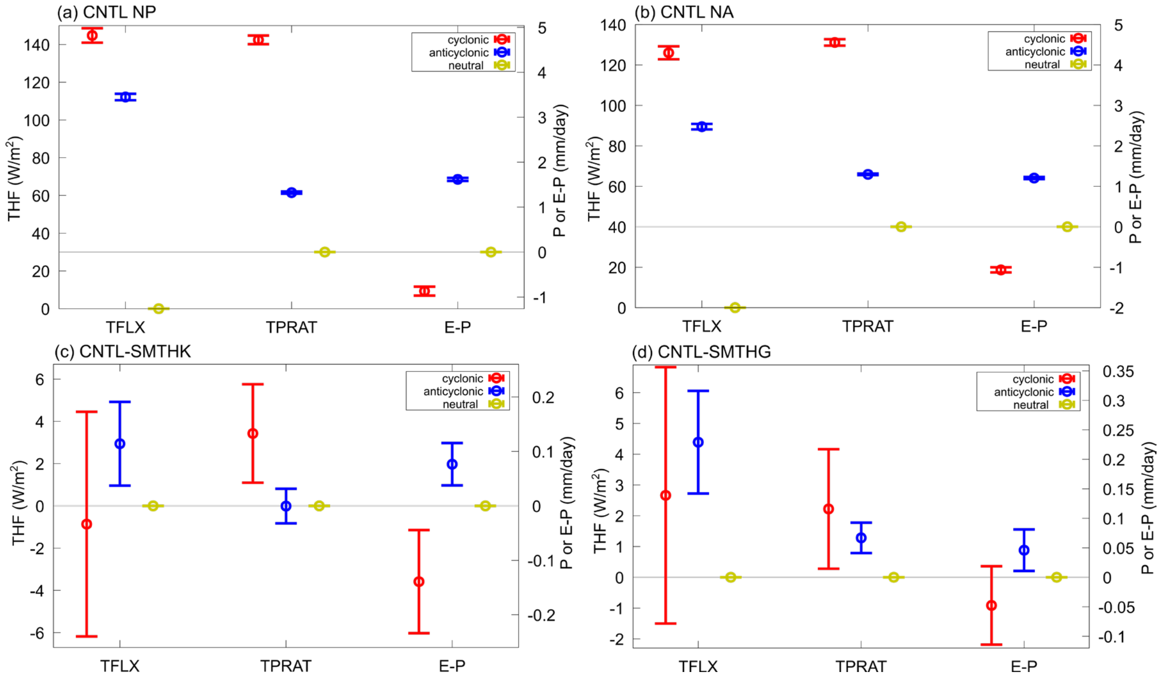

Figure S1. Same as in Fig. 3, respectively, but for the results based on a curvature threshold of zero.

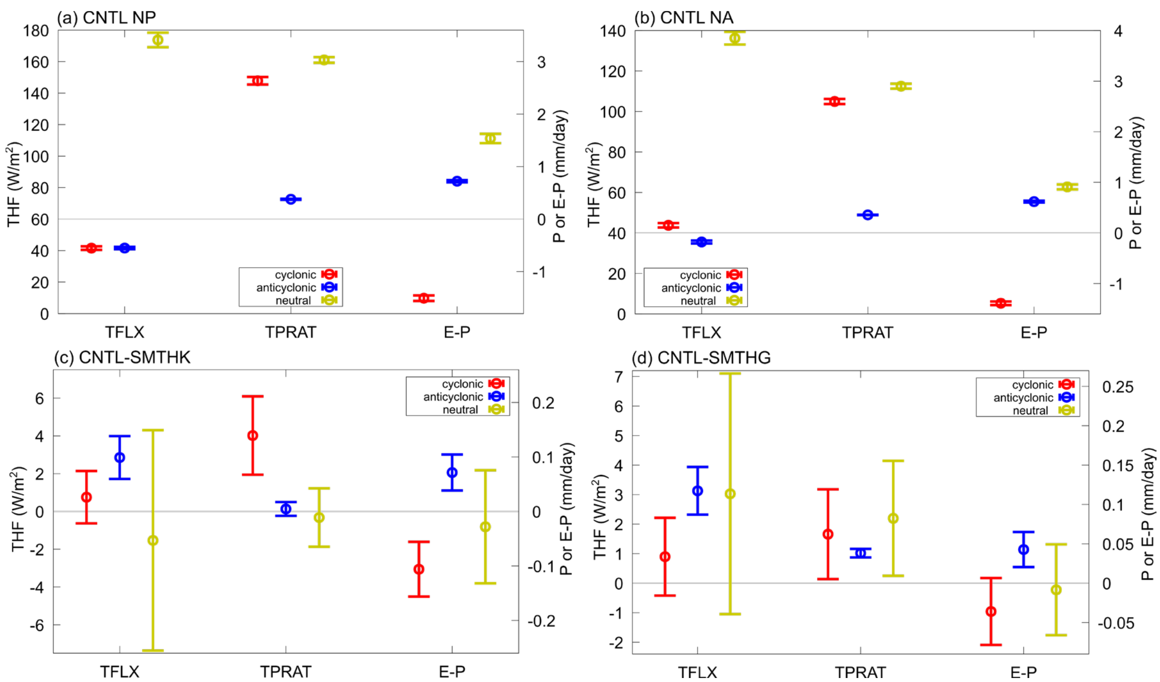

Figure S2. Same as in Fig. 3, respectively, but for the results based on a curvature threshold of $\pm 1.0 \times 10^{-6}$ m^{-1}, corresponding to a curvature radius of 1,000km.

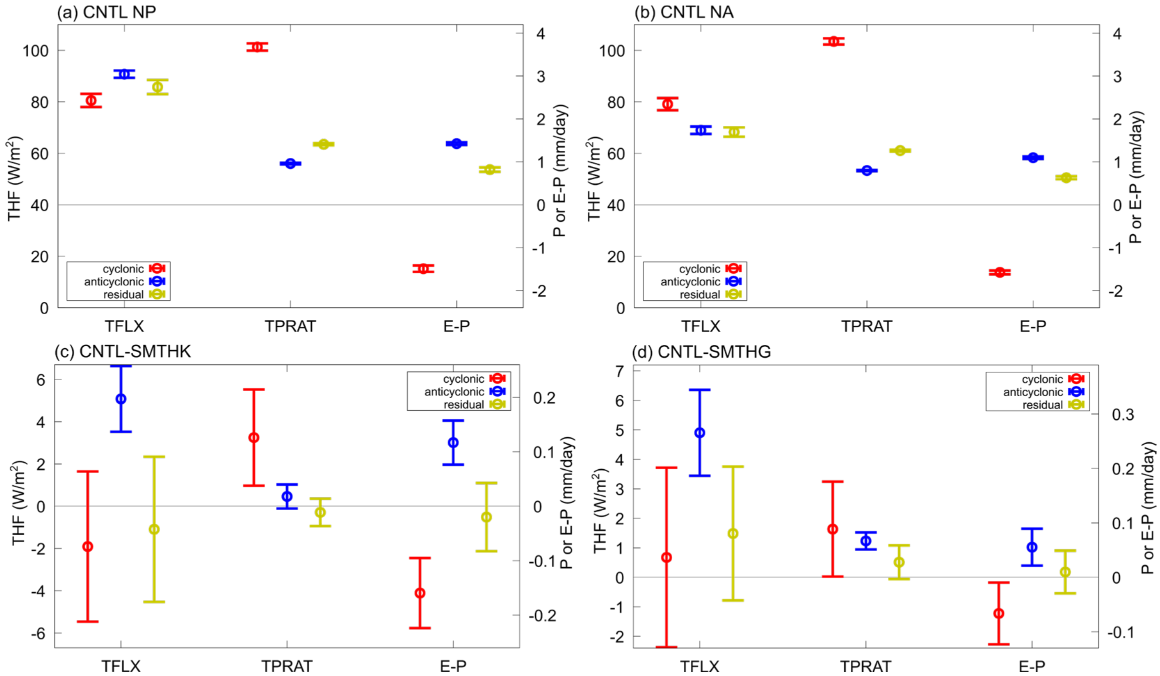

Figure S3. Same as in Fig. 3, respectively, but for the results based on the curvature of 925-hPa winds.

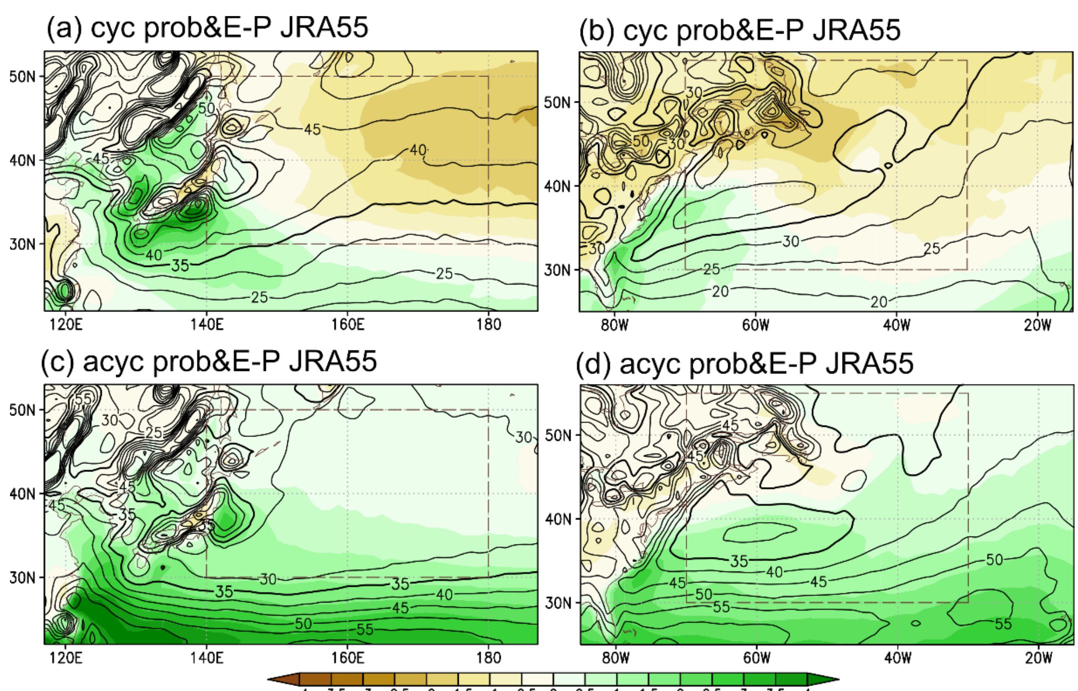

Figure S4. Same as in Figs. 1c-f, respectively, but for the results based on the JRA-55 reanalysis.

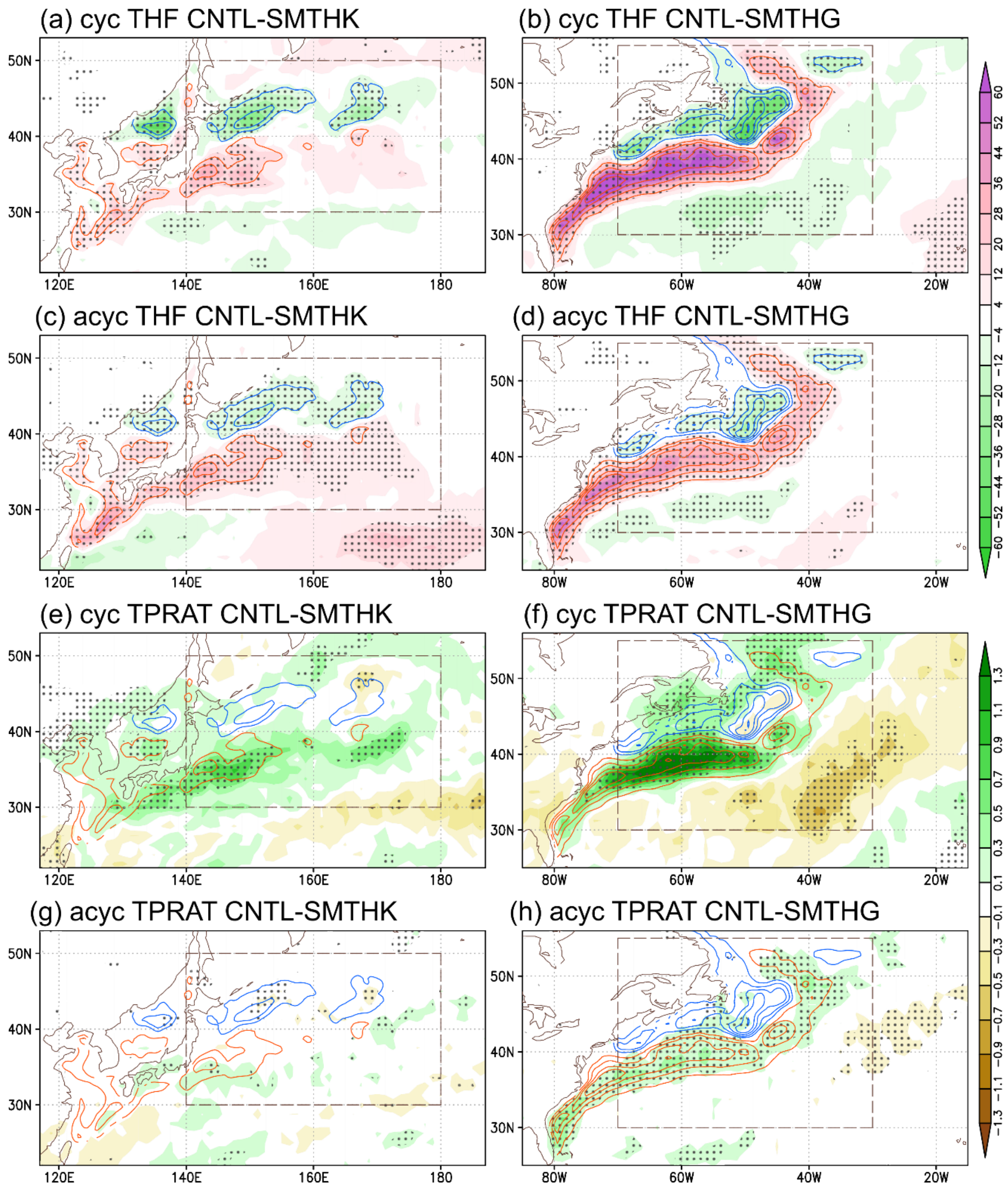

Figure S5. a-b Difference in climatological-mean wintertime net turbulent heat flux (black contours, W/m^2) between CNTL and SMTHK (CNTL–SMTHK) for (a) cyclonic and (b) anticyclonic contributions. Stipples denote statistically significant signals at 90% confidence level by Student's *t*-test. Red and blue contours indicate regions of warmer and colder SST (every 1K, zero contour omitted) in CNTL compared to SMTHK. **c-d** As panels a-b, respectively, but for total precipitation (mm/day). **e-h** As panels a-d, respectively, but for the differences between CNTL and SMTHG (CNTL–SMTHG). Dashed boxes signify the domains used to calculate the area-averaged contributions for the NP and NA, respectively.

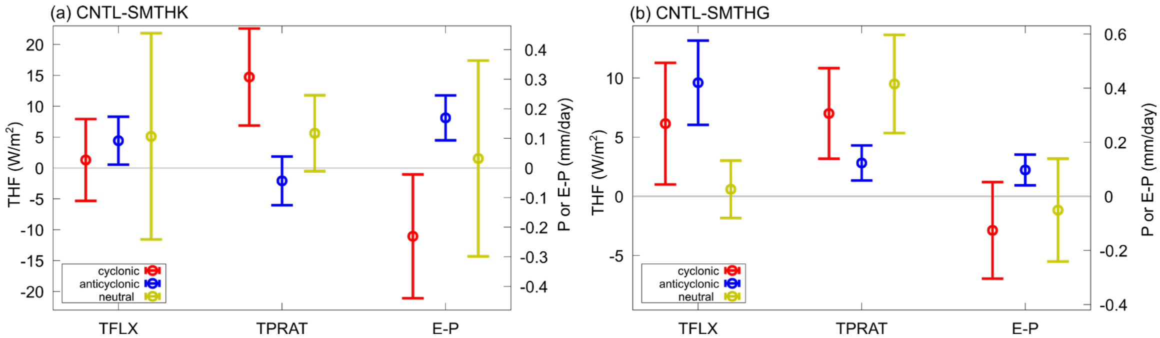

Figure S6. Same as in Figs. 3a-b, respectively, but for the results based on the JRA-55 reanalysis.

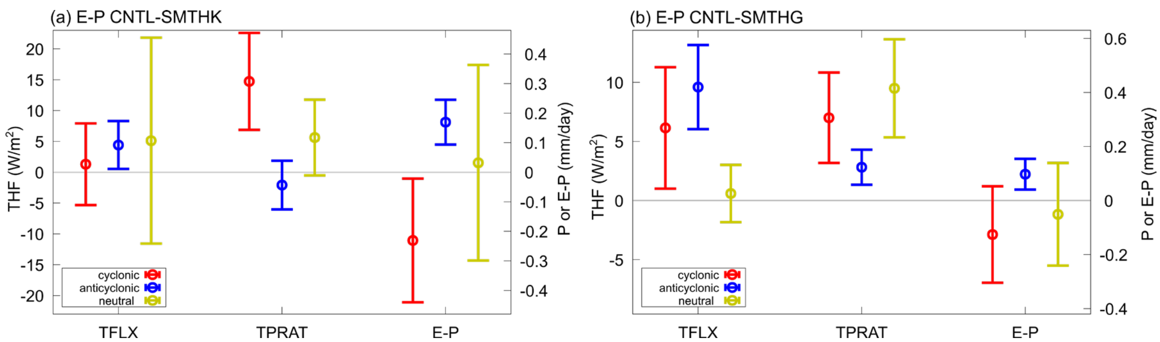

Figure S7. Same as in Fig. 3c-d, respectively, but for the results normalized by the corresponding probabilities of domains at 850-hPa for individual seasons.

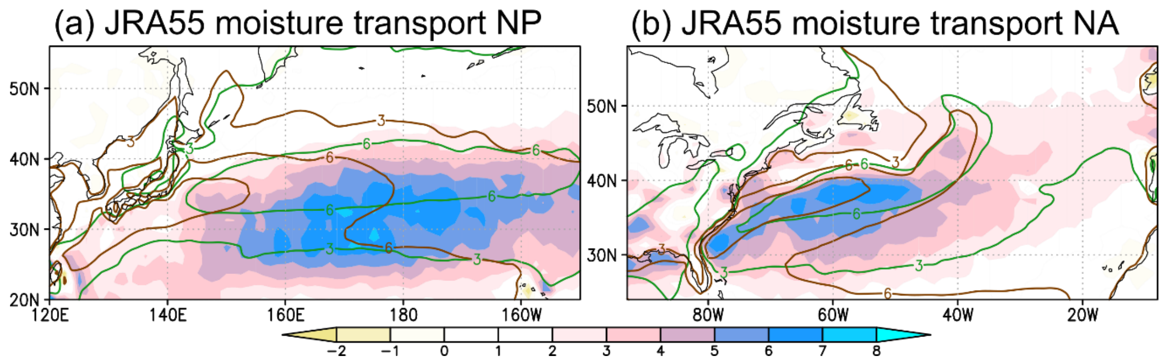

Figure S8. Same as in Figs. 4a-b, respectively, but for the results based on the JRA-55 reanalysis.

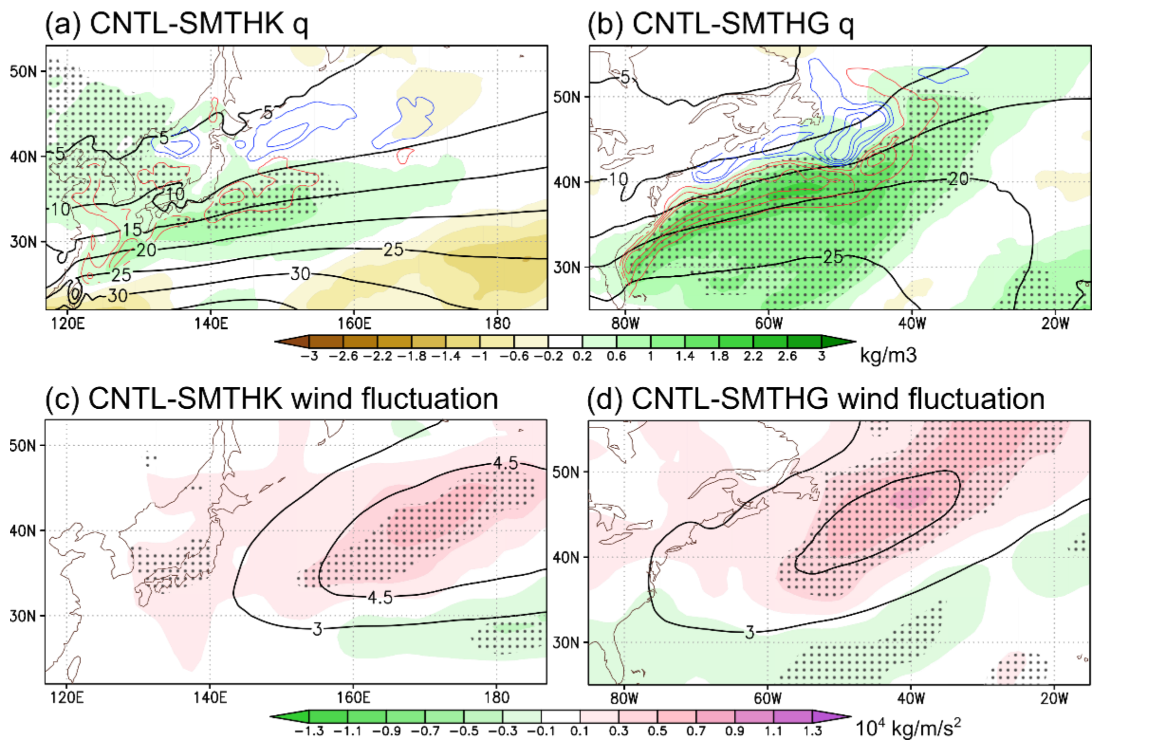

Figure S9. a Total response (CNTL–SMTHK) of the climatological specific humidity (shadings in kg/m^3) integrated vertically from the surface to 100-hPa. Stipples signify statistically significant signals at 90% confidence levels by Student's *t*-test. Contours denote vertically-integrated climatological specific humidity (kg/m^3) in CNTL. **b** Same as in (a), but for the total response of CNTL–SMTHG. **c-d** Same as in a-b, but for the variance of high-pass-filtered wind fluctuation projected onto the upgradient direction of local curvature (shadings in 10^4 kg/m/s^2; see Text S2 for details) integrated vertically from the surface to 700-hPa. In a-b, red and blue contours indicate regions of warmer and colder SST (every 1K, zero contour omitted) in CNTL compared to SMTHK or SMTHG.